Wetting and Contact Lines of Micrometer-Sized Ellipsoids

J. C. Loudet,[1] A. G. Yodh,[2] and B. Pouligny[1]

[1]*Centre de Recherche Paul Pascal, Avenue A. Schweitzer 33600 Pessac, France*

[2]*Department of Physics and Astronomy, University of Pennsylvania, Philadelphia, Pennsylvania 19104-6396, USA*

(Received 25 April 2006; published 7 July 2006)

We experimentally and theoretically investigate the shapes of contact lines on the surfaces of micrometer-sized polystyrene ellipsoids at the water-air interface. By combining interferometry and optical trapping, we directly observe quadrupolar symmetry of the interface deformations around such particles. We then develop numerical solutions of the partial wetting problem for ellipsoids, and use these solutions to deduce the shapes of the corresponding contact lines and the values of the contact angles, $_c(k)$, as a function of the ellipsoid aspect ratio k. Surprisingly, $_{c\psi}$is found to decrease for increasing $k\psi$ suggesting that ellipsoid microscopic surface properties depend on ellipsoid aspect ratio.

DOI: 10.1103/PhysRevLett.97.018304 PACS numbers: 82.70.Dd, 68.05.Cf, 68.03.Cd

Small objects located at the interface between two fluids interact *via* a variety of forces, either direct, such as colloidal Derjaguin-Landau-Verwey-Overbeek interaction potential (DLVO) interactions [1], or indirect, such as through deformations of the interface. Forces of the latter category, called ''capillary forces,'' affect objects over a very broad range of sizes, from nano to centimeters. Capillary deformations, for example, affect the aggregation of bubbles and colloidal particles at the air-water interface [2], and facilitate membrane-induced interactions of proteins in living cells [3,4]. Typically, two distant particles interact when each ''feels'' the interface deformation caused by the other. The interaction can be attractive or repulsive, and, of course, greater deformations produce stronger interactions [4].

Perhaps the simplest problem along these lines is that of a smooth sphere in deep water at the water-air interface. The condition of a constant contact angle $_{c\psi}$produces a plane circle contact line. If the particle is small enough—e.g., less than 0.1 mm—gravitational effects are negligible [2,4], and the interface remains flat around the contact line, thereby ruling out capillary interactions between such particles [5]. Deformations around small spheres arise in shallow water or in thin films and give rise to the well known ''immersion forces'' [3,4].

The ''smooth sphere,'' however, is an exceptional situation in nature. Nonideal surfaces and nonspherical shapes cannot accommodate planar contact lines [4,6–9]; consequently, surface deformations abound around realistic floating particles and the accompanying capillary interactions are common.

Recently, Danov *et al.* [9] reported a theoretical analysis of the problem of nonideal spheres, whose surfaces were rough or chemically heterogeneous, and thus induced the formation of distorted contact lines. They showed that the distortions of a circular contact line can be decomposed into a series of ''capillary multipoles,'' and they computed corresponding capillary force profiles. In this Letter, we return to the situation of an ideally smooth and homogeneous surface, but we focus on the *role of particle shape* in determining nonplanar contact lines. Specifically, we address the problem of an ellipsoid, through experiments with micrometer-sized polystyrene ellipsoidal particles, and by computation of the partial wetting configurations of such systems. The work provides first optical observations and measurements of the water-air interface deformation around floating ellipsoids, and then relates these experimental deformation fields to computed shapes of contact lines.

Prolate ellipsoids were obtained by uniaxial stretching of monodisperse polystyrene (PS) spheres (radius $R =$ 5 m, Polysciences) essentially following the method of [10]. The aspect ratio, defined as $k = a/b$, was varied from 1 (i.e., a sphere) to 10 (i.e., a rodlike particle). The long ($2a$), and short ($2b$) axes ranged from 11 to 45 m and from 4.5 to 9 m, respectively. In a recent Letter [11], it was shown that such ellipsoids at oil-water interfaces exhibit strong long-range interactions of up to 10^5 times thermal energy. The interactions were absent or much weaker for spherical particles, suggesting that the interaction between ellipsoids was induced *via* nonplanar contact lines. It was further observed that the interaction forces were anisotropic. In this Letter, we provide direct and quantitative information about the sources of these interactions.

The experimental setup is sketched in Fig. 1. The sample is prepared from a very dilute suspension of ellipsoids in a water-ethanol (1:1 vol.) mixture. A drop of the suspension is spread on a water-air interface (over a 2 cm^2 surface area) in a small cylindrical glass cell. The interface is viewed through an optical microscope, which incorporates optical trapping and a Michelson interferometer. Images are captured by video microscopy.

The optical trap uses a moderately focused beam from an Argon Ion laser (operating at 514 nm). The beam is mechanically scanned by means of an oscillating plate to provide an effective line trap, whose size is tuned to approximately match the ellipsoid length. The resulting

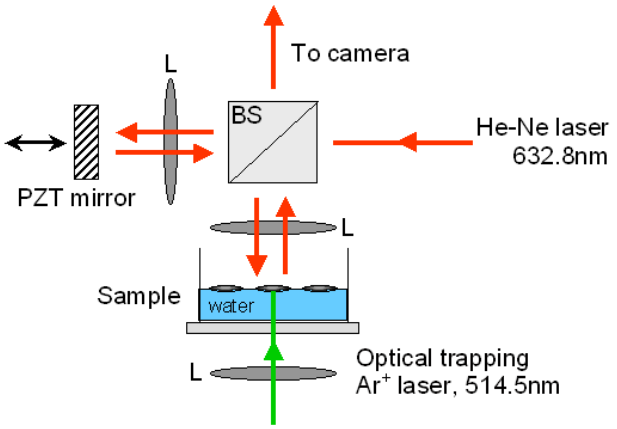

FIG. 1 (color online). Optical setup.

radiation pressure forces enable us to grab a single ellipsoid, fixing its position and angular orientation. This precaution is necessary because of spurious convection currents which otherwise make the particle rotate and drift out of the microscope field of view within a few seconds. Figure 2(a) shows a photo of an immobilized particle in white light illumination and simple transmission mode.

The interferometer, fed by a He-Ne laser (wavelength = 633 nm), is operated in reflection mode. Following the principles of "phase shifting interferometry" (PSI) [12], the mirror of the reference arm is mounted on a piezoelectric tube (PZT), allowing us to modulate the optical phase difference ( ) between the reference and signal arms over a few interference orders with a nanometric accuracy. Examples of interferograms are displayed in Figs. 2(b)–2(d), obtained from three successive positions of the reference mirror separated by $\lambda/8$, corresponding to a $\pi/2$ shift in . The motion of the mirror is synchronized with the CCD camera, meaning that a three-image PSI sequence, such as in Figs. 2(b)–2(d), is acquired in 0.12 s. The two-dimensional phase distribution, (x, y), in a single image is readily deduced from the PSI sequence, using a standard inversion procedure [12]. The height of the water-air interface at point (x, y) is simply given by $h(x, y) =$ $(x, y)/4$ and our corresponding height resolution is approximately 50 nm. In the remainder of this Letter, we only provide data about $h(x, y)$ outside of the particle contour. That is, we only account for the interference between the reference wave and light reflected by the water-air interface; added contributions that arise from solid-air and solid-water interfaces complicate the analysis inside the particle contour.

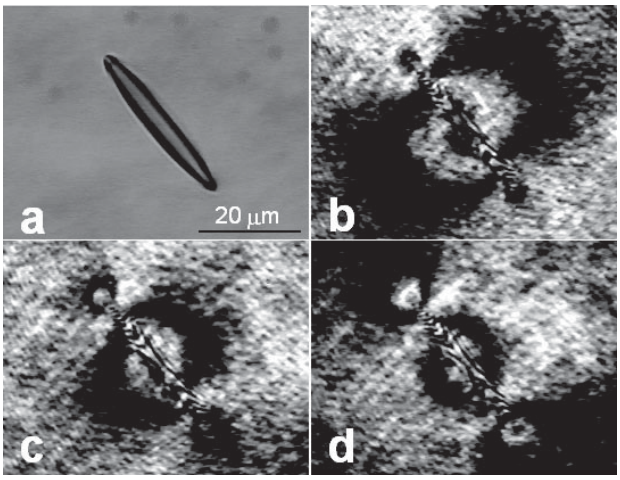

FIG. 2. (a) Optically trapped isolated ellipsoid ($k = 6.9$). (b)–(d) Typical PSI sequence (see text).

The interferograms (Fig. 2) clearly show that the water-air interface is not flat around the particle. Note the characteristic quadrupolar symmetry of the intensity patterns, in agreement with what might be expected by supposing the surface of the particle is smooth [13]. A color coded representation of the corresponding $h(x, y)$ is shown in Fig. 3(a). It is apparent that the interface is pulled down near the tips of the ellipsoid and pulled up near the middle of the particle. The altitude difference, Δh_p, is about 650 nm in this example. Recall that Δh_p is measured along the particle contour, not along the contact line itself, which is well within the contour.

These trends are observed only with ellipsoids, as can be verified from a control experiment with single spheres. The sphere example displayed in Fig. 3(b) shows that the interface around the sphere is flat to within the experimental noise. Similar observations were made over a range of different particles, i.e., spheres and ellipsoids with different aspect ratios. The data confirm the surfaces of the particles are smooth, giving circular (and flat, consequently) contact lines for $k = 1$ (spheres), and saddle-shaped contact lines for $k > 1$ (ellipsoids). Note, "smoothness" is defined only

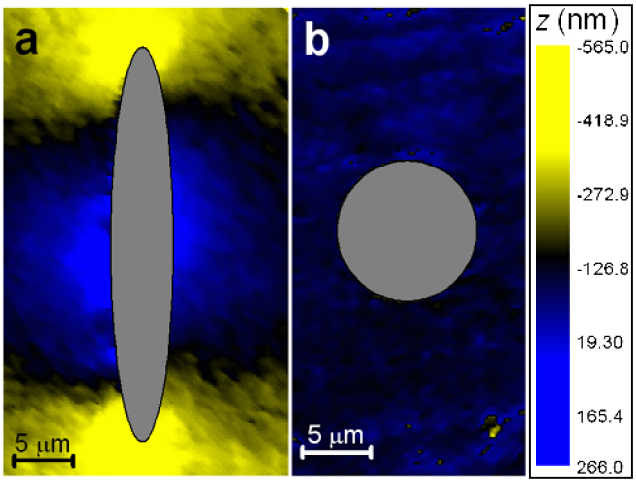

FIG. 3 (color online). Experimental image plots of the interfacial distortions $z = h(x, y)$ around floated particles calculated from PSI sequences. (a) Ellipsoid. (b) Sphere. The particle bodies were artificially colored in gray.

to be within the finite resolution of the PSI procedure (50 nm). The distortion of the interface increases with increasing k, as illustrated hereafter.

We thus find that the dominant interfacial deformations are driven by particle shape rather than by surface heterogeneity. The saddlelike distortion field explains previously observed interaction patterns between floating ellipsoids [11,14], wherein two such particles were observed to attract each other either tip to tip or side to side, and to repel each other in the side-to-tip configuration. These trends are also consistent with a general rule that interactions between capillary charges of same (opposite) sign are attractive (repulsive) [3,4].

We now come to the problem of exploiting the interferometric data to derive a quantitative description of the contact lines. We assume the shape of the contact line is set by the $_c$ = const condition [15], where $_{c\psi}$ is the contact angle of water on the polystyrene particle surface [see Fig. 4(a)]. Note, in the case of an ellipsoid, a planar cut of the particle body yields an ellipse, which does not generally meet the $_{c\psi}$ = const condition [16]. Thus the contact line cannot be planar, except for $_{c\psi} = 90°$. We derive the distortion field and the shape of the contact line from solution of the Laplace equation of capillarity for the interface height, $\Delta h(x, y) = 0$ [7–9]. The latter was solved numerically using a boundary element method [17]. Basically, this method yields the deformation field around a given contact line, L. In our application, we start with an initial line, L_1, along which we compute the distribution of contact angles, denoted as $_{c\psi}(L_1)$. In general $_c(L_1)$ does not satisfy the $_{c\psi}$ = const condition. In the next step, the contact line is modified, i.e., slightly pulled down where $_c(L_1)$ is too small and pulled up in the opposite case. A new contact angle distribution is computed, and the iteration is repeated until the desired value of $_{c\psi}$ is reached within $\pm 0.06°$. (Note, systematic tests proving the solution is unique were not performed; a more detailed analysis along these lines will be presented in a forthcoming paper.)

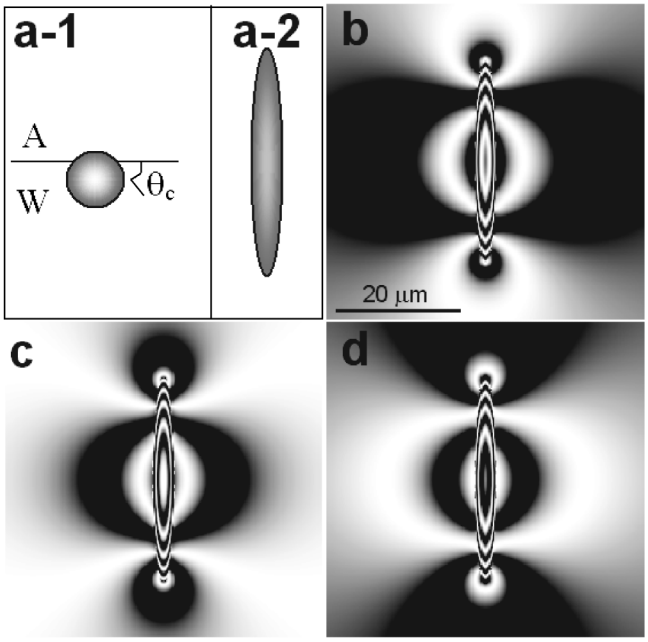

FIG. 4. (a-1) Definition of the contact angle $_{c\psi}$ (A: air; W: water). (a-2) Actual size of the ellipsoidal particle for the simulations in (b)–(d) ($k = 7$). (b)–(d) Simulation of a PSI sequence with $_{c\psi} = 39°$.

For given values of k and $_c$, we thus arrive at a solution contact line, $L(k, \psi_c)$, and the related deformation field. Results of the calculations are illustrated in Fig. 4, which shows a simulation of a PSI sequence for $R = 5$ m (as in the experiments) and $k = 7$. The comparison between the computational and experimental data, for a given k, amounts to finding the value of $_{c\psi}$ which provides the best fit of the computed PSI sequence to the experiment. The result of this procedure is shown for $k = 7$ in Fig. 4; for comparison with the experimental patterns, see Fig. 2. Note that the fringe patterns outside of the particle body, in the experiment [Figs. 2(b)–2(d)], and in the simulation [Figs. 4(b)–4(d)] are very similar, and therefore the deformation of the air-water interface is correctly represented by the model. We find $_{c\psi} = 39°$ in this example, within a $\pm 1°$ uncertainty.

We applied this procedure to the collection of PSI sequences recorded with particles of different k, yielding corresponding values of the contact angle $_{c\psi}(k)$ and of the altitude difference, $\Delta h_p(k)$. Recall that the latter corresponds to the difference between the highest and lowest points of $h(x, y)$ right outside of the particle contour. The simple expectation is that $_{c\psi}$ (and $\Delta h_p(k)$) should be nearly independent of k, since all the particles are made of the same material. Surprisingly, this expectation is definitely ruled out by the data analysis: no single value of the contact angle is found compatible with the measured variation of Δh_p with k. We instead find that $_{c\psi}$ is a decreasing function of k, following the trend shown in the inset of Fig. 5. The solid line in the main graph (curve 1) is the corresponding theoretical $\Delta h_p(k)$ function (normalized by R), which best reproduces the experimental tendency.

The variation of $_{c\psi}$ with k is paradoxical only if we assume that the surfaces of the ellipsoids are the same whatever the amount of stretching. The real situation is probably different. A tentative explanation is as follows: the value of the contact angle is an indication of the more or less hydrophilic character of the polystyrene particle surface, which itself is controlled by the surface concentration of ionic groups, . In the stretching procedure, the material is heated above the glass transition of polystyrene, allowing for the transformation of the sphere into an ellipsoid. If we suppose that the particle undergoes a purely plastic deformation, will be decreased as a consequence of the increase in surface area. However, the decrease should be much lower near the tips (where the dilation is lowest) than near the middle of the particle (where the dilation is high-

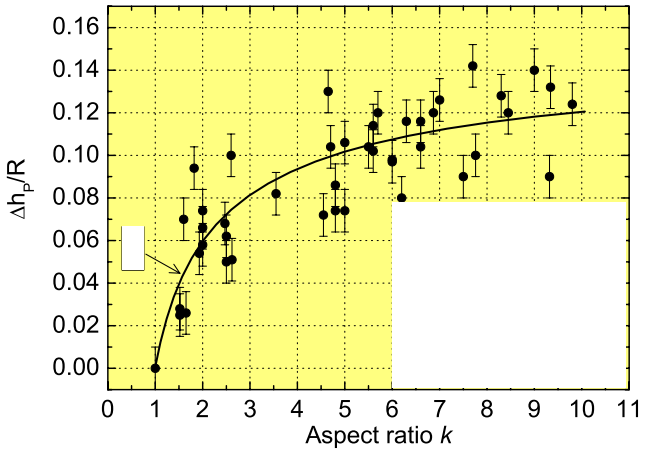

FIG. 5 (color online). Solid circles: experimental normalized deformations, $\Delta h_p/R$, as a function of aspect ratio k. Curve 1: calculated normalized deformations (see text). Inset: variation of $_{c\psi}$ with k deduced from curve 1 (see text).

est). Consequently, $_{c\psi}$ should be lower at the tips than near the middle, decreasing the amplitude of Δh_p, and resulting in an apparent decrease of the average $_c$. The effect should increase with increasing k, in line with the experimentally observed trend.

To conclude, we have explicitly shown that micrometer-sized polystyrene ellipsoids produce saddle-shaped contact lines, and thus that particle shape plays a vital role in the capillary force problem. However, the picture is more subtle than would be expected supposing aspect-ratio-independent properties.

We acknowledge partial support from the National Science Foundation (MRSEC No. DMR 05-20020 and No. DMR 05-05048) and we are grateful to the laboratory instrumentation team for their fruitful collaboration.

[1] W. B. Russel, D. A. Saville, and W. R. Schowalter, *Colloidal Dispersions* (Cambridge University Press, Cambridge, England, 1989).

[2] D. Vella and L. Mahadevan, Am. J. Phys. **73**, 817 (2005).

[3] P. A. Kralchevsky and N. D. Denkov, Current Opinion Colloid Interface Sci. **6**, 383 (2001).

[4] P. A. Kralchevsky and K. Nagayama, Adv. Colloid Interface Sci. **85**, 145 (2000).

[5] In principle, electric-field-induced deformations of a fluid interface are also possible. However, these are probably negligible in our experiments as can be seen from Fig. 3(b) where a "flat" interface is found for spheres. For details, see [18–22] below and K. D. Danov, P. A. Kralchevsky, and M. P. Boneva, Langmuir **22**, 2653 (2006).

[6] J. Lucassen, Colloids Surf. **65**, 131 (1992).

[7] D. Stamou, C. Duschl, and D. Johannsmann, Phys. Rev. E **62**, 5263 (2000).

[8] J. B. Fournier and P. Galatola, Phys. Rev. E **65**, 031601 (2002).

[9] K. D. Danov *et al.*, J. Colloid Interface Sci. **287**, 121 (2005).

[10] C. C. Ho *et al.*, Colloid Polym. Sci. **271**, 469 (1993).

[11] J. C. Loudet *et al.*, Phys. Rev. Lett. **94**, 018301 (2005).

[12] D. W. Robinson and G. T. Reid, *Interferogram Analysis* (Institute of Physics Publishing, England, 1993).

[13] Note the surface of latex particles is probably not smooth at the nanometer scale as shown by W. Chen *et al.*, Phys. Rev. Lett. **95**, 218301 (2005).

[14] A. B. D. Brown, C. G. Smith, and A. R. Rennie, Phys. Rev. E **62**, 951 (2000).

[15] E. A. Van Nierop, N. A. Stijnman, and S. Hilgenfeldt, Europhys. Lett. **72**, 671 (2005).

[16] D. R. M. Williams and E. Raphaël, J. Colloid Interface Sci. **155**, 509 (1993).

[17] C. Pozrikidis, *A Practical Guide to Boundary Element Methods* (Chapman & Hall/CRC, London, 2002).

[18] M. Megens and J. Aizenberg, Nature (London) **424**, 1014 (2003).

[19] L. Foret and A. Würger, Phys. Rev. Lett. **92**, 058302 (2004).

[20] M. Oettel, A. Dominguez, and S. Dietrich, Phys. Rev. E **71**, 051401 (2005).

[21] M. G. Nikolaides *et al.*, Nature (London) **420**, 299 (2002).

[22] T. S. Horozov *et al.*, Langmuir **21**, 7405 (2005) and references therein.